Regional Differences and Physiologic Behaviors in Peripapillary Scleral Fibroblasts

Julia Szeto,[1] Amanda Chow,[1] Liam McCrea,[1] Ann Mozzer,[1] Thao D. Nguyen,[1,4] Harry A. Quigley,[1,3] and Ian Pitha[1–3]

[1]Department of Ophthalmology, The Johns Hopkins University School of Medicine, Baltimore, Maryland, United States
[2]Center for Nanomedicine, The Johns Hopkins University School of Medicine, Baltimore, Maryland, United States
[3]Glaucoma Center of Excellence, The Johns Hopkins University School of Medicine, Baltimore, Maryland, United States
[4]Department of Mechanical Engineering, The Johns Hopkins University, Baltimore, Maryland, United States

Correspondence: Ian Pitha, Department of Ophthalmology, The Johns Hopkins University, Baltimore, MD 21218, USA; ipitha1@jhmi.edu.

Received: June 17, 2020
Accepted: December 18, 2020
Published: January 27, 2021

Citation: Szeto J, Chow A, McCrea L, et al. Regional differences and physiologic behaviors in peripapillary scleral fibroblasts. *Invest Ophthalmol Vis Sci.* 2021;62(1):27. https://doi.org/10.1167/iovs.62.1.27

Purpose. The purpose of this study was to describe the cellular architecture of normal human peripapillary sclera (PPS) and evaluate surface topography's role in fibroblast behavior.

Methods. PPS cryosections from nonglaucomatous eyes were labelled for nuclei, fibrillar actin (FA), and alpha smooth muscle actin (αSMA) and imaged. Collagen fibrils were imaged using second harmonic generation. Nuclear density and aspect ratio of the internal PPS (iPPS), outer PPS (oPPS), and peripheral sclera were determined. FA and αSMA fibril alignment with collagen extracellular matrix (ECM) was determined. PPS fibroblasts were cultured on smooth or patterned membranes under mechanical strain and in the presence of TGFβ1 and 2.

Results. The iPPS ($7.1 \pm 2.0 \times 10^{-4}$, $P < 0.0001$) and oPPS ($5.3 \pm 1.4 \times 10^{-4}$, $P = 0.0013$) had greater nuclei density (nuclei/μm^2) than peripheral sclera ($2.5 \pm 0.8 \times 10^{-4}$). The iPPS ($2.0 \pm 0.3$, $P = 0.002$) but not oPPS (2.4 ± 0.4, $P = 0.45$) nuclei had smaller aspect ratios than peripheral (2.7 ± 0.5) nuclei. FA was present throughout the scleral stroma and was more aligned with oPPS collagen (9.6 ± 1.9 degrees) than in the peripheral sclera (15.9 ± 3.9 degrees, $P = 0.002$). The αSMA fibers in the peripheral sclera were less aligned with collagen fibrils (26.4 ± 4.8 degrees) than were FA (15.9 ± 3.9 degrees, $P = 0.0002$). PPS fibroblasts cultured on smooth membranes shifted to an orientation perpendicular to the direction of cyclic uniaxial strain (1 Hz, 5% strain, 42.2 ± 7.1 degrees versus 62.0 ± 8.5 degrees, $P < 0.0001$), whereas aligned fibroblasts on patterned membranes were resistant to strain-induced reorientation (5.9 ± 1.4 degrees versus 10 ± 3.3 degrees, $P = 0.21$). Resistance to re-orientation was reduced by TGFβ treatment (10 ± 3.3 degrees without TGFβ1 compared to 23.1 ± 4.5 degrees with TGFβ1, $P < 0.0001$).

Conclusions. Regions of the posterior sclera differ in cellular density and nuclear morphology. Topography alters the cellular response to mechanical strain.

Keywords: extracellular matrix, collagen, surface topography, mechanical strain, myofibroblast

The sclera is an opaque tissue that forms approximately 85% of the outer shell of the eye.[1] Although the primary role of sclera – to protect the delicate vascular and neural tissues housed within the eye – seems simple, sclera must accomplish this goal under a constantly changing environment that includes variable loading conditions exerted by external factors, such as eye movement, and internal factors, such as variations in intraocular pressure (IOP) and ocular pulse pressure (OPP).[2] Scleral response to IOP level is relevant to glaucoma because it determines the IOP-induced stress and strain states in the optic nerve head (ONH) – an initial site of glaucomatous damage.[3]

Multiple lines of evidence implicate a role for scleral biomechanical behavior in causing axonal injury at the ONH in glaucomatous eyes. Sclera tissue adjacent to the ONH – the peripapillary sclera (PPS) – translates IOP-induced stress to the ONH and retinal ganglion cell axons[4] in ex vivo studies and finite element modeling.[5,6] Changes in the biomechanical properties of the PPS can alter the strain experienced by the lamina cribrosa (LC)[7] and the degree of axonal damage in animal models.[8] Glaucomatous sclera and LC have different mechanical characteristics than nondiseased tissue.[9] Scleral stiffening occurs following bead-induced murine glaucoma[10] and chronic IOP elevation in monkeys.[11] Postmortem human glaucomatous eyes are stiffer than nonglaucoma controls.[12] Scleral stiffening in monkey eyes is preceded by alterations in the viscoelastic properties of the peripapillary sclera that occur prior to axonal damage.[13] Changes in the mechanical behavior of sclera in animal models and glaucomatous human eyes are associated with alterations in collagen microarchitecture and extracellular matrix organization.[4,12,14] Taken together,

Table 1. Donor Information

Gender	Age	Race	Hours from Death to Fixation
M	76	Caucasian	35
M	56	Caucasian	34
F	97	Caucasian	37
M	77	Caucasian	34
M	77	Caucasian	36

these findings strongly suggest that factors that regulate scleral biomechanics are relevant to glaucoma pathogenesis.

The role of the main cellular component of the sclera – the fibroblast – in maintenance of scleral structure is not completely defined. The sclera is a paucicellular tissue that houses a population of largely dormant fibroblasts.[1] In experimental glaucoma eyes, scleral fibroblasts proliferate and increase expression of alpha smooth muscle actin (αSMA) and contractile proteins, such as myosin II, that signify an increase in scleral myofibroblasts.[15] These findings suggest that the cellular layers of the sclera are not static but adapt and respond to external stimuli to regulate extracellular matrix (ECM) properties in the setting of IOP stress. The bidirectional interaction between cells and ECM underlie diverse tissue remodeling and is known as dynamic reciprocity.[16,17] In order to further explore dynamic reciprocity in the sclera, it is necessary to gain a better understanding of cell-ECM interactions within the scleral stroma.

Here, we characterized previously unrecognized regional differences in scleral fibroblasts in the PPS and adjacent scleral tissue. Specifically, we found regional variations in cellular number, morphology, and alignment with extracellular collagen (as measured by second harmonic generation [SHG] imaging)[18] within the posterior scleral tissue. In parallel cultured fibroblast studies, we tested hypotheses that the scleral fibroblast response to cyclic stretch is influenced by extracellular topography.

Materials and Methods

Scleral Preservation, Sectioning, and Imaging

All experimental procedures involving human tissue were performed in accordance with the WMA Declaration of Helsinki on Ethical Principles for Medical Research Involving Human Subjects. Appropriate donor consents were obtained locally by eye banks. Donor details are included in Table 1. Eyes were obtained from the National Disease Research Interchange (NDRI, Philadelphia, PA, USA; Project Code DPII2 001 Protocol 003) within 24 hours of enucleation and immediately preserved. To ensure contact of fixative solution with all parts of the eye, two slits were cut through each globe on either side of the cornea at the limbus. Eyes were then placed into a jar and covered with a solution of 4% paraformaldehyde in 0.1 M Sorenson's phosphate buffer (Na_3PO_4, pH = 7.2). The jar was secured to a platform rocker and rocked at 4°C overnight. Supplementary Figure S1 illustrates eye dissection and sectioning. Briefly, after using anatomic landmarks to determine superior, inferior, temporal, and nasal aspects of the optic nerve head, the optic nerve, peripapillary sclera, and adjacent sclera were dissected (a 7–12 mm radius circle of tissue surround the optic nerve) and divided into superior, inferior, nasal, and temporal quarters prior to cryopreservation in sucrose and optimal cutting temperature compound (OCT; Sakura Finetek USA Inc., Torrance, CA, USA).

Cross-sections (16 µm) were cut parallel to the scleral surface and incubated in mouse anti-αSMA at 1:400 (Cat #A5228; Sigma-Aldrich, St. Louis, MO, USA) in Hanks' balanced salt solution (HBSS) with 0.5% Triton X-100 (HBT) and 10% normal goat serum (NGS; Jackson ImmunoResearch Laboratories, Inc., West Grove, PA, USA) overnight at 4°C. Slides were then washed in HBT and incubated with HBT with NGS, SYTOX Green at 1:30,000 (S7020; Thermo Fisher Scientific, Waltham, MA, USA), phalloidin Alexa Fluor 568 (Cat #A1280; Thermo Fisher Scientific), and goat anti-mouse Alexa Fluor 647 antibody at 1:200 (Cat #ab150115; Abcam, Cambridge, MA, USA). Slides were washed in HBT and coverslipped with Dako mounting media (Dako, Carpinteria, CA, USA). Imaging was performed on a Zeiss confocal laser scanning microscope 710 (Carl Zeiss Microscopy, LLC, Thornwood, NY, USA). SHG imaging was performed using the Zeiss 710 microscope with a coherent Chameleon Ultra II laser tuned to 780 nm and a 390 to 410 band pass filter. Laser power (2–20%) and gain (500–600) were adjusted to minimize oversaturated pixels. Images were stitched using ZEN 2.3 software (Carl Zeiss Microscopy) and converted to .tiff for image analysis.

Cell Counting and Morphology Analysis

Images were analyzed using ImageJ.[19] Three regions were delineated using the Region of Interest selection tool in ImageJ. These regions included an inner peripapillary scleral (iPPS) region that was 500 µm thick and adjacent to the optic nerve, an outer peripapillary scleral (oPPS) region adjacent to the iPPS that still had a circumferential collagen structure but was outside the iPPS, and a peripheral region adjacent to but outside of the oPPS in which a basket weave collagen orientation was present. Penetrating nerves and blood vessels were excluded from the regions of interest of all analyses. SYTOX green images were analyzed using the Shape Descriptors plugin with parameters 10 to 100 to quantify and characterize nuclei. The measure function was used to obtain the average pixel intensity value in peripapillary versus peripheral sclera.

Cellular-ECM and In Vitro Cellular Orientation Analysis

Analyses were performed on images labeled for fibrillar actin (FA) and αSMA, and on images using SHG delineation of collagen fibers. Supplementary Figure S2 provides an illustration of cellular-ECM orientation analysis. Vector fields were created using the Orientation J plugin of ImageJ using a Cubic Spline analysis with 32-pixel grid size and a 15-pixel local window (Supplementary Fig. S2a). Orientation J provided an output for FA, αSMA, and SHG images that included orientation (in degrees) and an intensity value for each vector. Vector fields were overlaid and difference in orientation between vectors (FA versus αSMA, FA versus collagen, and αSMA versus collagen) was calculated in degrees using the Orientation J output and MATLAB (The MathWorks Inc., Natick, MA, USA; Supplementary Fig. S2b) with 0 degrees indicated complete alignment and 90 degrees indicating perpendicular vectors. Heatmaps were created in MATLAB to illustrate orientation differences across vector fields with darker colors indicating less aligned vectors

Investigative Ophthalmology & Visual Science

(Supplementary Fig. S2c). Heatmaps showed alignment of up to 1024 separate 178 μm^2 zones per image set to demonstrate patterns of regional alignment. Prior to creation of heatmaps, low energy vectors associated with an image section without signal were excluded from the analysis by having a masked technician create an energy threshold that was applied to all vectors from a field. This step eliminated regions without signal from the final analysis; these regions appear black in the heatmaps. A global alignment score was calculated for each set of images by taking the mean value of each heatmap which contained 1024 (32 × 32) individual alignment values (Supplementary Fig. S2c).

Fibroblast Culture

Methods for isolation and culture of PPS were described previously in detail.[20] Donor eyes were obtained from the NDRI within 24 hours of enucleation. Lines were isolated from eyes of four European-derived persons without a clinical history of glaucoma or pathologic myopia: (1) an 80-year-old Caucasian woman, (2) a 79-year-old Caucasian man, left (3) and right (4) eyes from a 74-year-old Caucasian woman, and (5) a 56-year-old Caucasian man with no ocular history other than cataracts. Briefly, a 2-mm wide scleral band surrounding the ONH was isolated and cut into 1 by 1 mm sections. Sclera pieces were then placed on 35 mm collagen-coated, tissue culture dishes containing RPMI-1640 medium, 20% fetal bovine serum (FBS), nonessential amino acids, 1% penicillin/streptomycin, and sodium pyruvate. After 14 days, cells were passaged and cultured in Dulbecco's modified Eagle's medium (DMEM) with 10% FBS, 1% penicillin/streptomycin, and sodium pyruvate. All experiments were conducted on cells between passages 3 and 10.

Cyclic cellular strain experiments were conducted using a Nanosurface Cytostretcher (Nanosurface Biomedical Inc., Seattle, WA, USA) and collagen-coated chambers with topography in parallel with direction of strain or flat topography (Nanosurface Biomedical Inc.). Dimensions of the grooves and ridges of the parallel topography surface were 800 nm with a depth of 600 nm.[21] After seeding, PPS fibroblasts were allowed to settle for 48 hours in media containing 1% FBS prior to strain (5%, 1 Hz, 24 hours). TGFβ1 or TGFβ2 (R&D Systems, Minneapolis, MN, USA; 2 ng/mL) was added 1 hour prior to strain. Oregon Green binding assays for extracellular matrix production were performed as described previously.[22]

Fibroblast Orientation Analysis

Analysis was performed on light microscope images of cells taken using a 10 × objective lens on a Nikon Eclipse TS100 microscope (Nikon Inc., Melville, NY, USA) with a SPOT Insight digital camera (Diagnostic Instruments, Inc., Sterling Heights, MI, USA). At least 12 images were taken per chamber. Orientation was determined manually for each cell using the Measure function of ImageJ for at least 20 cells per image. Mean orientation was determined.

Statistical Analyses

All values are mean ± standard deviation (SD). Unless otherwise noted, means were compared using 1-way analysis of variance test (ANOVA) with Dunnett post hoc tests to correct for multiple comparisons. For in vitro cell culture experiments, cell lines from either four or five different donor eyes were used and at least three biologic samples were analyzed per group.

Results

Nuclear Density and Morphology Defines Distinct Peripapillary Regions

Initial analysis of imaging of nuclei revealed distinct regions within the PPS. The PPS region immediately adjacent to the optic nerve contained a greater density of cells when compared to more distal PPS. Therefore, we divided the PPS into an iPPS region of 500 μm width that was immediately adjacent to the optic nerve, an oPPS region that was immediately adjacent to the iPPS and retained circumferential collagen structure of the PPS. The outer limit of the oPPS and the beginning of the peripheral sclera was defined by the presence of basket weave collagen organization. The portion of each section in which a basket-weave collagen lamellar structure was present was defined as the peripheral region (Figs. 1a, 1b). Nuclear density was measured as nuclear counts/μm^2 and percent scleral area. Density was greatest in the iPPS, intermediate in the oPPS, and lowest in the peripheral sclera (Fig. 1c, Table 2). Nuclear aspect ratio was compared among the three regions and found to vary systematically, with rounder nuclear outlines in iPPS and more elongated profiles in oPPS and peripheral sclera, and this difference was significant between the iPPS and the peripheral sclera (aspect ratios of 2.0 ± 0.3 in iPPS versus 2.7 ± 0.5 in peripheral sclera, $P = 0.002$, $n = 5$ eyes; Fig. 1d).[2] An analysis of the PPS (iPPS and oPPS combined) and peripheral sclera was performed and is shown in Supplementary Figure S3. In this supplemental analysis, cellular density was significantly greater in the PPS versus peripheral sclera (in each nuclei/micron^2 and percent scleral area), however, there was not a significant difference in nuclear aspect ratio.

Processes Containing Fibrillar Actin are Present Throughout Scleral Stroma

FA staining revealed several findings. Despite seeming to be relatively paucicellular, scleral sections contained a dense network of FA processes (Fig. 2a), suggesting that each fibroblast sends many processes through the tissue. This network was present in all three regions – iPPS, oPPS, and peripheral. Interestingly, in the peripheral sclera the FA had a basket-weave pattern (Fig. 2b), whereas in the iPPS and oPPS, FA was arranged circumferentially (Fig. 2c). These regional patterns mirrored those of the scleral stromal collagen.[23] The dense nature of the FA network prevented visualization of individual fibroblast morphology.

FA is Aligned With Collagen Fibrils

We quantitatively characterized FA and collagen fibril alignment. In the present studies, we focused on the oPPS and peripheral regions. The iPPS region was not included as the presence of penetrating vessels and the small size of this region made alignment analysis inexact. This analysis permitted visualization of alignment throughout each scleral region by creating a heatmap with light blue indicating close alignment and dark blue indicating poor alignment (Figs. 3a, 3b) and a mean alignment value for each image set

Investigative Ophthalmology & Visual Science

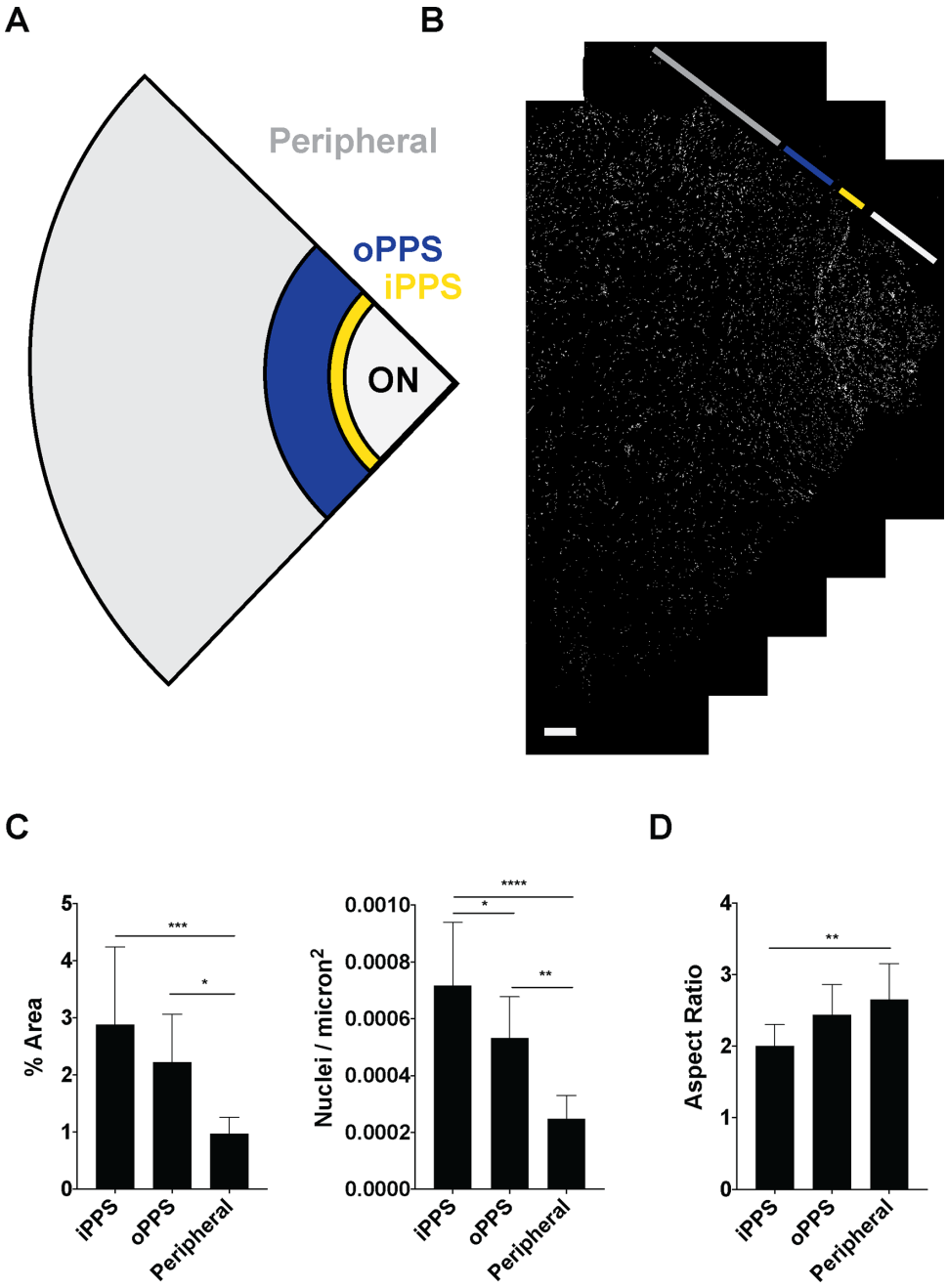

Figure 1. Greater nuclear density and rounder nuclei in PPS than peripheral sclera. (**A**) Schematic of scleral section indicating different regions, including optic nerve (ON, *white*), iPPS (*yellow*), oPPS (*blue*), and peripheral sclera (*grey*). (**B**) Image of scleral section stained for nuclei (*Sytox Green, white*) with ON, iPPS, oPPS, and peripheral sclera depicted (scale bar = 500 µm). (**C**) Nuclear density is increased, and aspect ratio is decreased in peripapillary regions compared to peripheral sclera (n = 5 eyes). *P < 0.05, **P < 0.01, ****P < 0.0001.

Table 2. Nuclear Density

	Region	Nuclear Counts/µm^2 × 10^{-4} (SD)	*P* Value		Region	% Scleral Area (SD)	*P* Value
a	iPPS	7.1 (2.2)	d-e (0.04)	d	iPPS	2.87 (1.4)	a-b (ns)
b	oPPS	5.3 (1.4)	e-f (0.001)	e	oPPS	2.12 (0.84)	b-c (0.02)
c	Peripheral	2.4 (0.81)	d–f (<0.0001)	f	Peripheral	0.97 (0.28)	a–c (0.0003)

ns, not significant.

that represented the overall FA-collagen alignment in each region. Both oPPS and peripheral sclera had a high degree of FA-collagen alignment, but that of the oPPS was significantly more aligned (Fig. 3c). Circumferentially patterned collagen and FA of the oPPS were more highly aligned, (mean angle = 9.6 ± 1.9 degrees) than the peripheral sclera

Investigative Ophthalmology & Visual Science

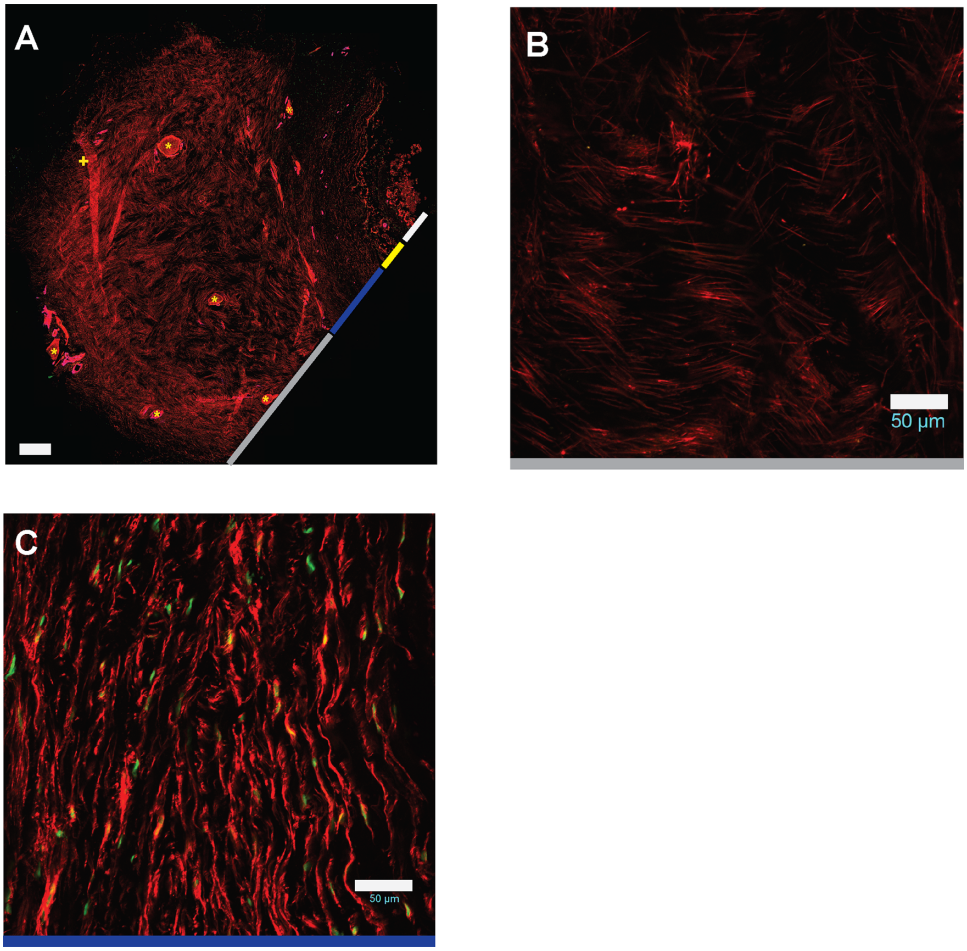

Figure 2. Fibrillar actin processes permeate scleral stroma. (**A**) FA staining (phalloidin, *red*) of scleral section including ON, iPPS, oPPS, and peripheral sclera (scale bar = 500 µm; + = fold; * = penetrating nerve or vessel). Higher magnification view of FA staining of (**B**) peripheral sclera and (**C**) oPPS shows basket weave and circumferential arrangements, respectively (scale bar = 50 µm).

(15.9 ± 3.9 degrees; difference from PPS, $P = 0.002$, $n = 5$ eyes), although the latter was still very aligned. The mean values were to some degree affected by regions of poor alignment that occurred around the many nerves and vessels that penetrate this region of the posterior sclera in both peripheral sclera and PPS. Exclusion from the analysis of areas adjacent to penetrating structures led to even greater degrees of alignment in both areas but did not eliminate the greater alignment in PPS (PPS = 7.6 ± 1.3 degrees, JPS = 11.1 ± 2.5 degrees, difference $P = 0.01$; Fig. 3d).

αSMA Expressing Cells are Found in Vascular and Stromal Structures

The αSMA labeling was seen in a small number of fibroblasts in the peripheral sclera and PPS (Fig. 4b, arrowheads). Higher magnification of αSMA-labeled fibroblasts within the peripheral sclera revealed multiple extensions originating from the cell body (Fig. 4c); this branched morphology was not seen in PPS fibroblasts. The αSMA-expressing fibrils that were not associated with cell bodies were seen throughout the stroma (Fig. 4b arrows and Fig. 4d). Additionally, αSMA labeling was prominent in walls of penetrating vessels and the central retinal artery, as expected (Fig. 4, asterist).

We hypothesized that fibroblasts expressing αSMA would have poorer alignment with collagen than FA from non-αSMA-expressing fibroblasts. Indeed, in the peripheral sclera, αSMA fibrils were significantly less aligned with collagen than FA (Fig. 5). Mean αSMA-collagen alignment was significantly poorer (greater in degrees) than that of FA-collagen (26.4 ± 4.8 degrees for αSMA-collagen versus 15.9 ± 3.9 degrees for FA-collagen, $P = 0.0002$, $n = 5$ eyes). Additionally, αSMA-collagen alignment was significantly less than αSMA-FA alignment (26.4 ± 4.8 degrees for αSMA-collagen versus 17.3 ± 5.8 degrees for αSMA-FA, $P = 0.005$). In the oPPS, there was not a significant difference between αSMA-collagen alignment (14.9 ± 3.6 degrees) and FA-collagen alignment (10.7 ± 3.1 degrees, $P = 0.09$, $n = 3$ eyes), although there was a trend toward lower αSMA-collagen alignment (Fig. 5b).

Topographic Cues Alter PPS Fibroblast Response to Mechanical Strain

Primary human PPS fibroblasts were cultured on membranes with a similar stiffness to human sclera[4] with either a smooth surface or a surface with parallel ridges to promote cell alignment. Cells were randomly oriented on flat membranes,

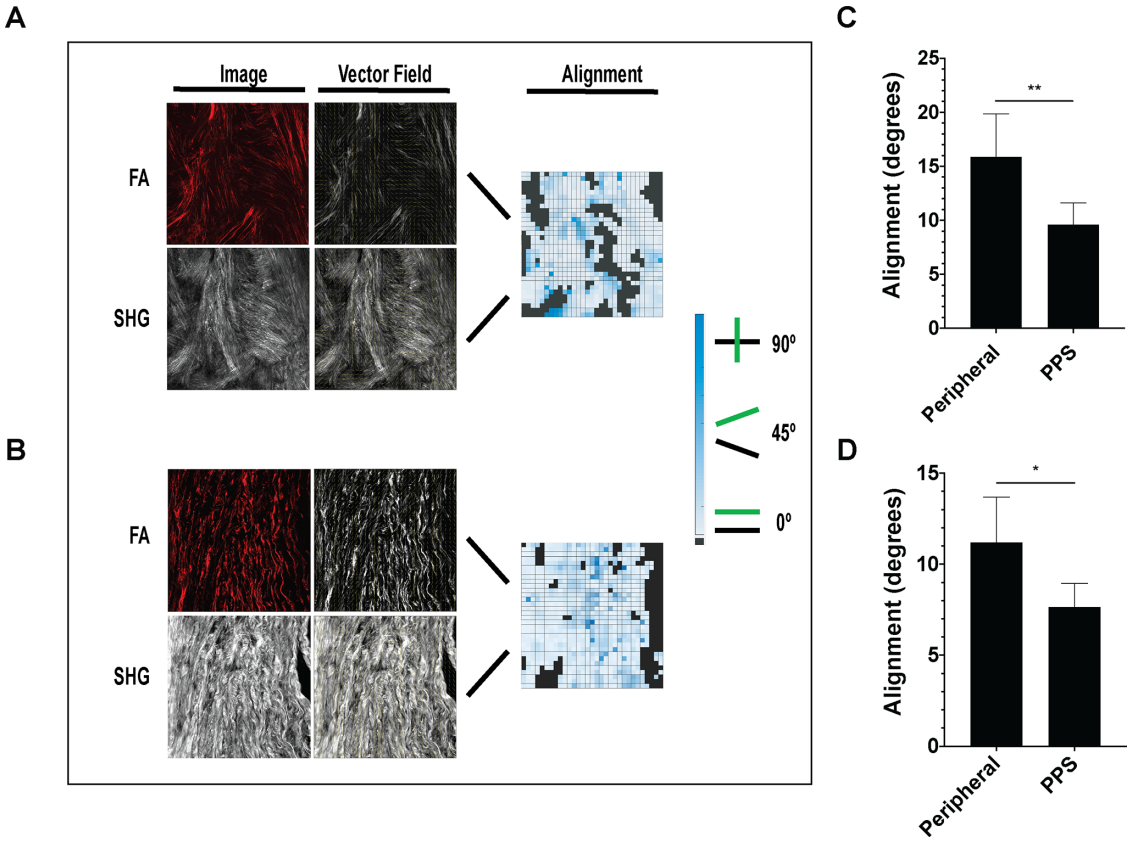

Figure 3. Greater FA-collagen alignment in oPPS than peripheral sclera. Examples of alignment analysis of (**A**) peripheral sclera and (**B**) oPPS with FA and SHG images, their corresponding vector fields, and alignment heat maps. *Darker blue* indicates poorer alignment and black boxes indicate points in which sufficient image signal was not present for analysis in either FA or SHG images. Reduced FA-collagen alignment in peripheral sclera versus oPPS in image sets that included (**C**) and excluded (**D**) areas adjacent to penetrated vessels and nerves.

but aligned parallel to the ridges in patterned membranes (Figs. 6a, 6b).[21] Cell orientations on the flat membrane were broadly distributed while orientation on patterned membranes were narrowly distributed parallel to the direction of the topographic grooves (Fig. 6c). The same cells were then exposed cyclic, uniaxial 5% strain at 1 Hz for 24 hours, and orientation was measured. These strain levels are consistent with tissue strain with IOP elevation[24]; while sclera is under constant variable strain in vivo we have validated that this frequency range elicits a fibroblast response and is within a physiologic range.[2] Uniaxial and not biaxial strain will be used because it models better the circumferential and compressive strain within the PPS[25] and allowed strain avoidance quantification. In this measure, 90 degrees indicates an orientation perpendicular to direction of strain and 0 degrees indicates an orientation parallel to the strain. Fibroblasts on flat membranes shifted to an orientation perpendicular to the direction of strain (42.2 ± 7.1 degrees in no strain versus 62.0 ± 8.5 degrees with strain, $P < 0.0001$; Fig. 7a). This shift in orientation by fibroblasts under cyclic stress was described previously on flat membranes and is known as strain avoidance.[26] By contrast, fibroblasts cultured on patterned membranes remained in their orientation parallel to membrane ridges after 24 hours of cyclic strain (5.9 ± 1.4 degrees without strain versus 10 ± 3.3 degrees with strain, $P = 0.21$, $n = 5$ cell lines; Fig. 7b).

In sclera stroma, we found that αSMA-expressing myofibroblasts had processes with reduced alignment with surrounding collagen. Therefore, we hypothesized that myofibroblasts in culture would exhibit reduced alignment with surrounding topography. To test this hypothesis, fibroblasts were seeded on parallel topography membranes, treated with TGFβ1 or TGFβ2 at a concentration that induced myofibroblast differentiation (2 ng/mL),[20] and exposed to cyclic uniaxial strain. Prior to performing these experiments, we demonstrated TGFβ2-induced SMA expression and extracellular matrix production is slightly reduced compared to TGFβ1-iduced effects (Supplementary Fig. S4). TGFβ-treated cells on the patterned membrane were aligned in the absence of strain (5.9 ± 1.4 degrees without TGFβ1 treatment versus 9.5 ± 2.5 degrees with TGFβ1, $P = 0.30$, $n = 5$ cell lines; and 7.8 ± 2.6 degrees without TGFβ2 treatment versus 5.6 ± 2.0 degrees with TGFβ2, $P = 0.86$, $n = 4$ cell lines; see Fig. 7b). When TGFβ-treated cells were placed under uniaxial cyclic strain, alignment with parallel grooves was reduced and shifted even further toward an orientation perpendicular to the direction of the applied strain (10.0 ± 3.3 degrees with TGFβ1 and no strain versus 23.1 ± 4.5 degrees with TGFβ1 and strain, $P < 0.0001$, $n = 5$ cell lines; and 6.72 ± 2.3 degrees with TGFβ2 and no strain versus 19.3 ± 7.0 degrees with TGFβ2 and strain, $P = 0.002$, $n = 4$ cell lines; see Fig. 7b).

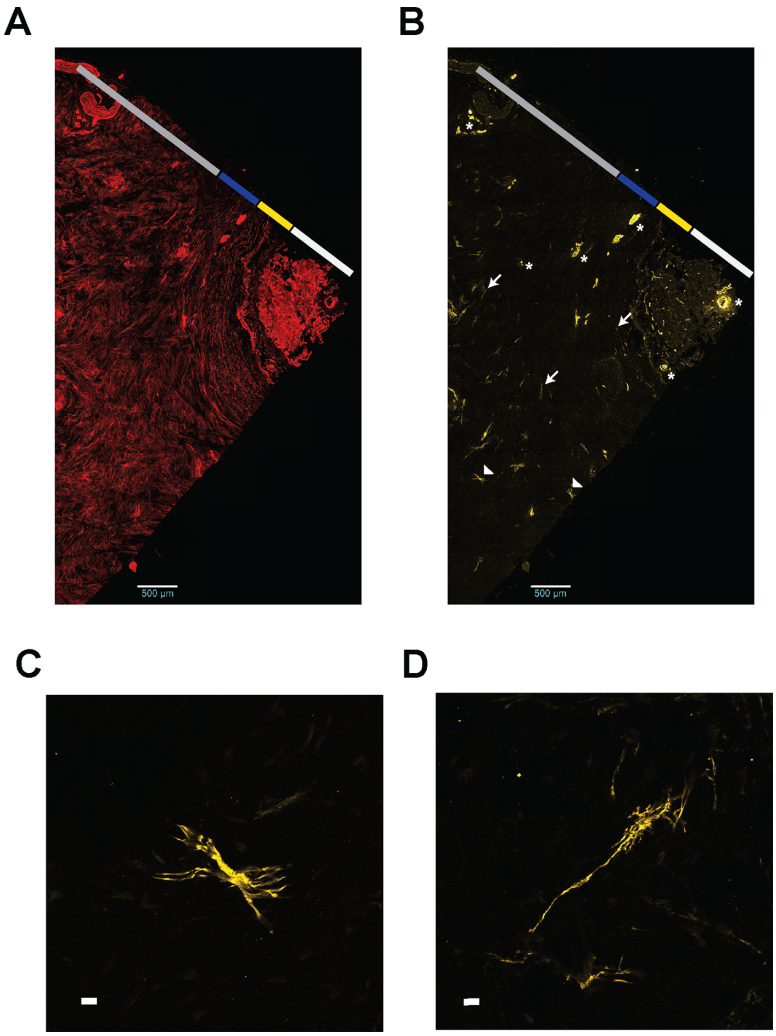

Figure 4. Scleral αSMA expression occurs in a small number of stromal fibroblasts. FA (**A**) and αSMA (**B**) in the same scleral section. The αSMA expression is highlighted in vessels (*), fibrils (*arrows*), and stromal cells (*arrowheads*; scale bar = 500 µm). The central retinal artery is far right of **A** and **B**. Higher magnification view of αSMA-expression cell body (**C**) and fibril (**D**) (scale bar = 25 µm).

Discussion

Here, we describe three main findings regarding the cellular architecture of scleral fibroblasts and translate these results to an in vitro system that investigates the significance of surface topography on the behavior of scleral fibroblasts under mechanical strain. First, we describe novel cellular niches within the sclera consisting of an iPPS and oPPS with increased density of cells and rounder cells than peripheral regions. Second, FA was visible throughout the sclera and was highly aligned with surrounding ECM. Last, αSMA expression occurred in a subset of scleral stromal cells and αSMA fibrils exhibited reduced alignment with surrounding collagen when compared to FA-collagen alignment. We additionally describe an in vitro system that demonstrated two key features of scleral fibroblast behavior: (1) topographic cues alter the way in which scleral fibroblasts respond to mechanical strain, and (2) TGFβ – treatment alters scleral fibroblast response to the combination of topographic cues and mechanical strain.

PPS and peripheral sclera contained distinct cellular niches with different cellular density and nuclear morphology. Previous work has described a lamellar and connected cellular architecture of mouse scleral fibroblasts using transmission electron microscopy (TEM) and immunofluorescent microscopy.[15,27,28] This work did not differentiate differences in cellular density or morphology based of anatomic location. Evidence of distinct fibroblast niches was also described in isolated primary human[29] and mouse[30] scleral fibroblasts, however, these findings were not correlated to location. Here, we identified scleral regional specialization by examining nuclear density and morphology in the iPPS, oPPS, and peripheral sclera. Interestingly, there are distinct cellular niches within the scleral stroma. These niches correspond to previously described regions of collagen architecture. The peripheral sclera contains collagen oriented in a basket-weave pattern and the stromal nuclei within this region are less densely packed and rounder than nuclei within PPS regions. We additionally noted distinct cellular niches within the PPS with the iPPS having a greater density of nuclei than the oPPS. Differences in collagen crimp were noted previously in the iPPS and oPPS regions of sheep eyes.[31] Although we did not use an imaging technique that measured collagen crimp, this finding does further support

Investigative Ophthalmology & Visual Science

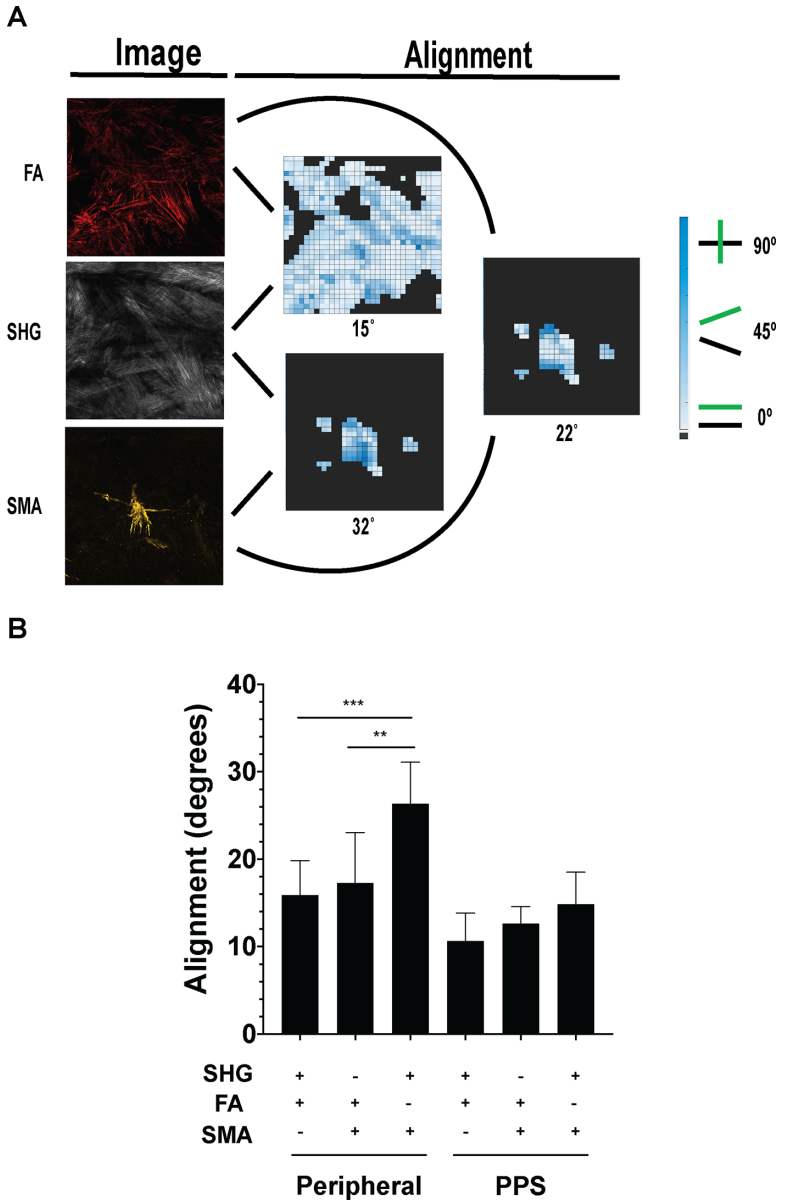

Figure 5. The αSMA-collagen alignment is reduced in peripheral sclera but not PPS. (**A**) Alignment analysis of FA and αSMA with collagen (SHG) with mean alignment values placed under each heatmap. (**B**) αSMA and FA alignment with collagen in peripheral sclera (*left*) and PPS (*right*).

the hypothesis that collagen structure influences cellular behavior and creates niches of cells with distinct characteristics within the sclera.

An additional delineation of cellular niches in the PPS and peripheral sclera occurs between stromal areas and penetrating structures, such as the optic nerve head and its accompanying vessels, the short and long posterior ciliary arteries, circle of Zinn-Haller, and the short and long ciliary nerves with their accompanying vessels. These penetrating cellular structures add to the cellular diversity of the PPS and peripheral sclera and need to be considered as contributing factors in any experiments investigated the proteomic or RNA composition of the PPS.

Imaging of scleral FA and its relation to collagen using SHG revealed two novel findings. First, collagen and cytoskeletal FA structures are highly aligned. Additionally, FA and collagen were highly aligned in PPS and to a lesser extent in the peripheral sclera. Whether this degree of alignment is persistent through all scleral structures, changes with age, is susceptible to racial variation, or is altered in disease states, such as glaucoma or pathologic myopia, are all potential areas of future study. The linkage between FA and collagen occurs at focal adhesion complexes (FACs) that contain clusters of membrane integrins that link the ECM to intracellular structures that regulate cellular cytoskeletal structure, nuclear structure, and gene expression.[32] The organization of these linkages – in combination with topographic cues – regulate cytoskeletal organization, cell morphology, and allow cells to sense and react to extracellular signals, such as mechanical strain and tissue stiffness.[21] How alterations in glaucomatous sclera ECM are caused by or affect FAC and cytoskeletal organization is not known and is a topic of future study.

Investigative Ophthalmology & Visual Science

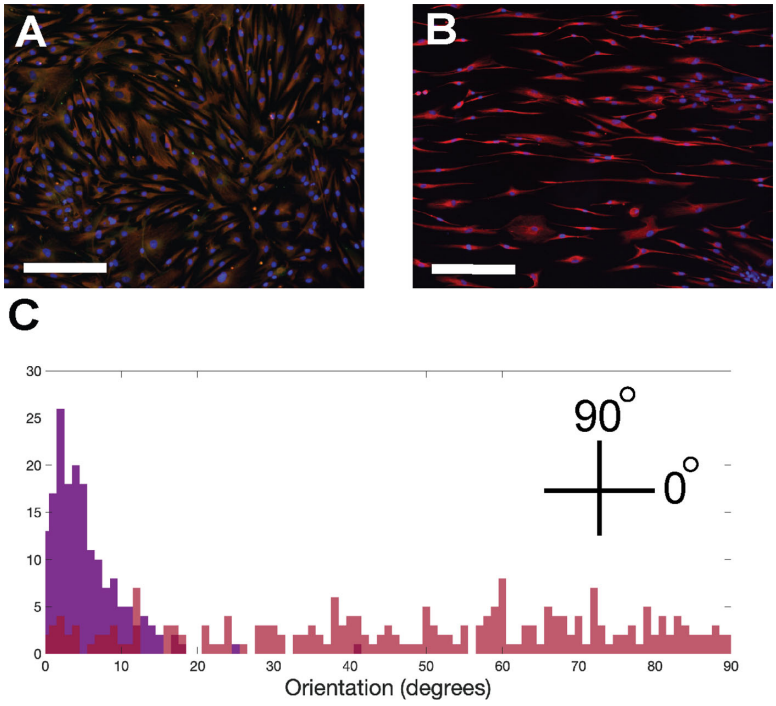

Figure 6. Topographic cues align cells. Immunofluorescence imaging of PPS fibroblasts on smooth membrane (**A**) and on of fibroblasts on patterned surface topography with horizontally oriented grooves (**B**) (scale bar = 275 µm; *red* = FA, *blue* = DAPI). Frequency distribution of cellular orientation of cells on flat (*red*) and patterned (*purple*) membranes.

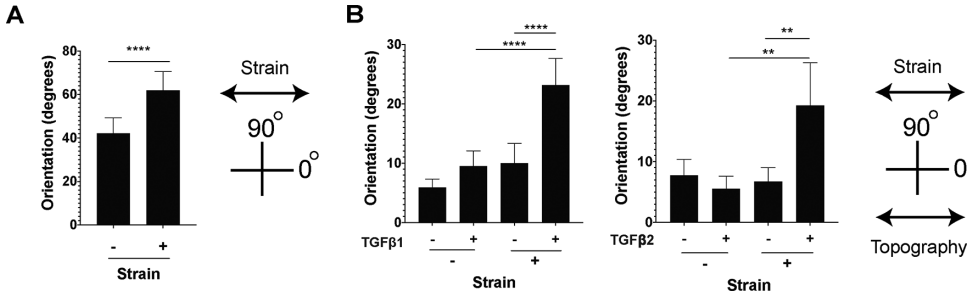

Figure 7. Topographic cues and TGFβ-treatment alter response to mechanical strain. (**A**) Cellular orientation on flat smooth membranes with and without cellular strain. (**B**) Cellular strain orientation on patterned membranes with and without TGFβ1 or 2 (2 ng/mL for 24 hours) treatment.

The role of αSMA expression by scleral fibroblasts in normal and disease sclera is of considerable interest. The αSMA expressing fibroblasts were described in human and primate sclera,[33] as well as in animal models of IOP glaucoma[15] and myopia.[30] Here, we describe focal stromal αSMA expression in a subset of peripheral and PPS fibroblasts. The αSMA-expressing fibroblasts have contractile activity and are present in areas of tissue remodeling and fibrosis.[34] Although scleral contraction was described previously following IOP elevation in the chick and tree shrew eye,[35] it is unlikely that these cells are present in abundant enough numbers to acutely or subacutely alter scleral shape in humans. It is more likely that these cells are involved in chronic scleral remodeling processes. The role of αSMA expressing cells in ECM remodeling and fibrosis is well described, as are many of the signals that increase and sustain αSMA expression.[34,36] These signals, which include mechanical strain and signaling molecules, such as TGFβ, are present in sclera and enriched in glaucomatous eyes.[2,37] The role of αSMA expressing cells in glaucomatous scleral remodeling is not completely known; however, they are increased in glaucomatous eyes. Treatments that antagonize TGFβ activity alter glaucomatous scleral remodeling in a murine model of IOP glaucoma.[38] Our findings demonstrate a subset of αSMA expressing cells in nonglaucomatous eyes suggesting that these cells could be involved in normal scleral homeostasis as well and highlight the need to further explore the role of these cells in scleral function and remodeling.

Our findings additionally highlight the relevance of the role of extracellular topography in regulating scleral fibroblast and αSMA-expressing fibroblast activity. Previous studies examined the behavior of cultured scleral fibroblasts on flat surfaces exposed to biaxial strain.[24,29,39] Here, we described cellular alignment in scleral stroma and showed that extracellular topography affects fibroblast activity in

Investigative Ophthalmology & Visual Science

vitro. Previous studies described a cellular behavior coined the strain avoidance phenomenon in which cells placed under uniaxial strain reorient to a position perpendicular to the direction of the applied strain.[40] The ability of topographic cues to prevent reorientation is influenced by strain characteristics (amount, frequency, and duration) as well as topographic features.[41,42] Our in vitro findings indicate that topographic cues can stabilize fibroblasts by preventing a change in cellular orientation in the presence of mechanical strain. These cues could play a similar role in stabilizing fibroblasts in scleral tissue under IOP-induced strain. Loss of normal topography, resistance to topographic cues (through TGFβ exposure), or pharmacologic manipulation of the cytoskeletal response to ECM topography could alter scleral fibroblast response to environmental signals and initiate a cycle of pathologic remodeling. Our findings suggest that two hits are needed to alter fibroblast migratory behavior: (1) induction of myofibroblast differentiation and (2) mechanical strain. Perhaps altering the fibroblast response to these signals could block the cycle of pathologic scleral remodeling that occurs in glaucomatous eyes. We have shown previously inhibition of ECM-cytoskeletal signaling pathways, such as rho-kinase or src-kinase signaling, alters fibroblast response to IOP elevation.[20,22] Future studies should evaluate scleral fibroblast signaling and behavior in the presence of topographies that resemble scleral collagen.

The present study has some recognized limitations. Although the lamellar organization of scleral tissue allowed characterization of cellular architecture and collagen alignment in two-dimensions, we do not characterize the three-dimensional architecture of the sclera, its cells, their nuclei, or the alignment of cytoskeleton and collagen. In addition, eyes examined were all from Caucasian donors over 50 years old. Future studies should examine sclera from a wider age range of donors with different racial backgrounds. Last, whereas the stiffness of material used in cell culture experiments was similar to that of human sclera, the ridges of the patterned topography are significantly larger than that of collagen fibrils.[22,23] Therefore, we are unable to make a direct correlation between in vitro and in vivo cell behavior.

Conclusions

In summary, we describe imaging studies of the cellular architecture of the PPS and peripheral sclera. Our studies identified novel cellular niches within the iPPS, oPPS, and peripheral sclera. Further examination showed a high degree of alignment of extracellular collagen and cytoskeletal FA. Additionally, we found a subset of αSMA-expressing stromal fibroblasts with reduced alignment to ECM collagen. We then demonstrated that extracellular topographic cues alter cellular response to mechanical strain. Future studies will examine the cellular components of glaucomatous sclera and the role of extracellular topography on regulating scleral fibroblast behavior.

Acknowledgments

Supported in part by PHS research grants EY 02120 (H.Q.) and EY001765 (Wilmer Institute Core grant). I.P. was supported by a RPB Career Development Award (I.P.). The funders had no role in study design, data collection and analysis, decision to publish, or preparation of the manuscript.

Disclosure: **J. Szeto**, None; **A. Chow**, None; **L. McCrea**, None; **A. Mozzer**, None; **T.D. Nguyen**, None; **H.A. Quigley**, None; **I. Pitha**, None

References

1. Boote C, Sigal IA, Grytz R, Hua Y, Nguyen TD, Girard MJA. Scleral structure and biomechanics [published online ahead of print August 11, 2019]. *Prog Retin Eye Res*, https://doi.org/10.1016/j.preteyeres.2019.100773.
2. Turner DC, Edmiston AM, Zohner YE, et al. Transient intraocular pressure fluctuations: source, magnitude, frequency, and associated mechanical energy. *Invest Ophthalmol Vis Sci*. 2019;60(7):2572–2582.
3. Quigley HA, Addicks EM, Green WR, Maumenee AE. Optic nerve damage in human glaucoma. II. The site of injury and susceptibility to damage. *Arch Ophthalmol*. 1981;99(4):635–649.
4. Coudrillier B, Tian J, Alexander S, Myers KM, Quigley HA, Nguyen TD. Biomechanics of the human posterior sclera: age- and glaucoma-related changes measured using inflation testing. *Invest Ophthalmol Vis Sci*. 2012;53(4):1714–1728.
5. Sigal IA, Flanagan JG, Ethier CR. Factors influencing optic nerve head biomechanics. *Invest Ophthalmol Vis Sci*. 2005;46(11):4189–4199.
6. Sigal IA, Flanagan JG, Tertinegg I, Ethier CR. Finite element modeling of optic nerve head biomechanics. *Invest Ophthalmol Vis Sci*. 2004;45(12):4378–4387.
7. Thornton IL, Dupps WJ, Sinha Roy A, Krueger RR. Biomechanical effects of intraocular pressure elevation on optic nerve/lamina cribrosa before and after peripapillary scleral collagen cross-linking. *Invest Ophthalmol Vis Sci*. 2009;50(3):1227–1233.
8. Kimball EC, Nguyen C, Steinhart MR, et al. Experimental scleral cross-linking increases glaucoma damage in a mouse model. *Exp Eye Res*. 2014;128:129–140.
9. Liu B, McNally S, Kilpatrick JI, Jarvis SP, O'Brien CJ. Aging and ocular tissue stiffness in glaucoma. *Surv Ophthalmol*. 2018;63(1):56–74.
10. Nguyen C, Cone FE, Nguyen TD, et al. Studies of scleral biomechanical behavior related to susceptibility for retinal ganglion cell loss in experimental mouse glaucoma. *Invest Ophthalmol Vis Sci*. 2013;54(3):1767–1780.
11. Girard MJ, Suh JK, Bottlang M, Burgoyne CF, Downs JC. Biomechanical changes in the sclera of monkey eyes exposed to chronic IOP elevations. *Invest Ophthalmol Vis Sci*. 2011;52(8):5656–5669.
12. Coudrillier B, Pijanka JK, Jefferys JL, et al. Glaucoma-related changes in the mechanical properties and collagen micro-architecture of the human sclera. *PLoS One*. 2015;10(7):e0131396.
13. Downs JC, Suh JK, Thomas KA, Bellezza AJ, Hart RT, Burgoyne CF. Viscoelastic material properties of the peripapillary sclera in normal and early-glaucoma monkey eyes. *Invest Ophthalmol Vis Sci*. 2005;46(2):540–546.
14. Pijanka JK, Coudrillier B, Ziegler K, et al. Quantitative mapping of collagen fiber orientation in non-glaucoma and glaucoma posterior human sclerae. *Invest Ophthalmol Vis Sci*. 2012;53(9):5258–5270.
15. Oglesby EN, Tezel G, Cone-Kimball E, et al. Scleral fibroblast response to experimental glaucoma in mice. *Mol Vis*. 2016;22:82–99.
16. Bissell MJ, Aggeler J. Dynamic reciprocity: how do extracellular matrix and hormones direct gene expression? *Prog Clin Biol Res*. 1987;249:251–262.
17. Bissell MJ, Hall HG, Parry G. How does the extracellular matrix direct gene expression? *J Theor Biol*. 1982;99(1):31–68.

18. Chen X, Nadiarynkh O, Plotnikov S, Campagnola PJ. Second harmonic generation microscopy for quantitative analysis of collagen fibrillar structure. *Nat Protoc*. 2012;7(4):654–669.
19. Rueden CT, Schindelin J, Hiner MC, et al. ImageJ2: ImageJ for the next generation of scientific image data. *BMC Bioinformatics*. 2017;18(1):529.
20. Pitha I, Oglesby E, Chow A, et al. Rho-kinase inhibition reduces myofibroblast differentiation and proliferation of scleral fibroblasts induced by transforming growth factor beta and experimental glaucoma. *Transl Vis Sci Technol*. 2018;7(6):6.
21. Tabdanov ED, Puram V, Zhovmer A, Provenzano PP. Microtubule-actomyosin mechanical cooperation during contact guidance sensing. *Cell Rep*. 2018;25(2):328–338.e5.
22. Chow A, McCrea L, Kimball E, Schaub J, Quigley H, Pitha I. Dasatinib inhibits peripapillary scleral myofibroblast differentiation. *Exp Eye Res*. 2020;194:107999.
23. Pijanka JK, Spang MT, Sorensen T, et al. Depth-dependent changes in collagen organization in the human peripapillary sclera. *PLoS One*. 2015;10(2):e0118648.
24. Qu J, Chen H, Zhu L, et al. High-magnitude and/or high-frequency mechanical strain promotes peripapillary scleral myofibroblast differentiation. *Invest Ophthalmol Vis Sci*. 2015;56(13):7821–7830.
25. Midgett DE, Pease ME, Jefferys JL, et al. The pressure-induced deformation response of the human lamina cribrosa: analysis of regional variations. *Acta Biomater*. 2017;53:123–139.
26. Chagnon-Lessard S, Jean-Ruel H, Godin M, Pelling AE. Cellular orientation is guided by strain gradients. *Integr Biol (Camb)*. 2017;9(7):607–618.
27. Cone-Kimball E, Nguyen C, Oglesby EN, Pease ME, Steinhart MR, Quigley HA. Scleral structural alterations associated with chronic experimental intraocular pressure elevation in mice. *Mol Vis*. 2013;19:2023–2039.
28. Murata K, Hirata A, Ohta K, Enaida H, Nakamura KI. Morphometric analysis in mouse scleral fibroblasts using focused ion beam/scanning electron microscopy. *Sci Rep*. 2019;9(1):6329.
29. Qiu C, Chen M, Yao J, et al. Mechanical strain induces distinct human scleral fibroblast lineages: differential roles in cell proliferation, apoptosis, migration, and differentiation. *Invest Ophthalmol Vis Sci*. 2018;59(6):2401–2410.
30. Wu H, Chen W, Zhao F, et al. Scleral hypoxia is a target for myopia control. *Proc Natl Acad Sci USA*. 2018;115(30):E7091–E7100.
31. Jan NJ, Gomez C, Moed S, et al. Microstructural crimp of the lamina cribrosa and peripapillary sclera collagen fibers. *Invest Ophthalmol Vis Sci*. 2017;58(9):3378–3388.
32. Alexander J, Cukierman E. Stromal dynamic reciprocity in cancer: intricacies of fibroblastic-ECM interactions. *Curr Opin Cell Biol*. 2016;42:80–93.
33. Poukens V, Glasgow BJ, Demer JL. Nonvascular contractile cells in sclera and choroid of humans and monkeys. *Invest Ophthalmol Vis Sci*. 1998;39(10):1765–1774.
34. Hinz B. Myofibroblasts. *Exp Eye Res*. 2016;142:56–70.
35. Phillips JR, McBrien NA. Pressure-induced changes in axial eye length of chick and tree shrew: significance of myofibroblasts in the sclera. *Invest Ophthalmol Vis Sci*. 2004;45(3):758–763.
36. Hinz B. The myofibroblast: paradigm for a mechanically active cell. *J Biomech*. 2010;43(1):146–155.
37. Pena JD, Taylor AW, Ricard CS, Vidal I, Hernandez MR. Transforming growth factor beta isoforms in human optic nerve heads. *Br J Ophthalmol*. 1999;83(2):209–218.
38. Quigley HA, Pitha IF, Welsbie DS, et al. Losartan treatment protects retinal ganglion cells and alters scleral remodeling in experimental glaucoma. *PLoS One*. 2015;10(10):e0141137.
39. Yuan Y, Li M, To CH, et al. The role of the RhoA/ROCK signaling pathway in mechanical strain-induced scleral myofibroblast differentiation. *Invest Ophthalmol Vis Sci*. 2018;59(8):3619–3629.
40. Kaunas R, Nguyen P, Usami S, Chien S. Cooperative effects of Rho and mechanical stretch on stress fiber organization. *Proc Natl Acad Sci USA*. 2005;102(44):15895–15900.
41. Wang Q, Huang H, Wei K, Zhao Y. Time-dependent combinatory effects of active mechanical loading and passive topographical cues on cell orientation. *Biotechnol Bioeng*. 2016;113(10):2191–2201.
42. Wang JH, Grood ES. The strain magnitude and contact guidance determine orientation response of fibroblasts to cyclic substrate strains. *Connect Tissue Res*. 2000;41(1):29–36.

Investigative Ophthalmology & Visual Science